AFRL-OSR-VA-TR-2013-0628

(HBCU/MI) TUNABLE INFRARED SEMICONDUCTOR LASERS

STEVEN BRUECK

UNIVERSITY OF NEW MEXICO

12/20/2013
Final Report

AIR FORCE RESEARCH LABORATORY
AF OFFICE OF SCIENTIFIC RESEARCH (AFOSR)/RSE
ARLINGTON, VIRGINIA 22203
AIR FORCE MATERIEL COMMAND

REPORT DOCUMENTATION PAGE

Form Approved
OMB No. 0704-0188

1. REPORT DATE *(DD-MM-YYYY)*	**2. REPORT TYPE**	**3. DATES COVERED** *(From - To)*
19-12-2013	Final	1/9/2010-31/8/2013

4. TITLE AND SUBTITLE

Tunable Infrared Semiconductor Lasers

5a. CONTRACT NUMBER

5b. GRANT NUMBER

FA9550-10-1-0517

5c. PROGRAM ELEMENT NUMBER

6. AUTHOR(S)

Brueck, S. R. J.

5d. PROJECT NUMBER

5e. TASK NUMBER

5f. WORK UNIT NUMBER

7. PERFORMING ORGANIZATION NAME(S) AND ADDRESS(ES)

University of New Mexico
1700 Lomas Blvd. Ste 2200
Albuquerque, NM 87106-3804

8. PERFORMING ORGANIZATION REPORT NUMBER

9. SPONSORING / MONITORING AGENCY NAME(S) AND ADDRESS(ES)

Air Force Office of Scientific Research
875 North Randolph Street, Rm 3112
Arlington, VA 22203

10. SPONSOR/MONITOR'S ACRONYM(S)

AFOSR

11. SPONSOR/MONITOR'S REPORT NUMBER(S)

12. DISTRIBUTION / AVAILABILITY STATEMENT

Unrestricted

13. SUPPLEMENTARY NOTES

14. ABSTRACT

An 80 nm continuous tuning range has been demonstrated on a large area index-coupled, optically pumped mid-infrared type-II semiconductor distributed feedback (DFB) laser, with a typical spectral linewidth of ~1.2 nm and 820 mW single facet output power. Different from other methods to widely tune the laser output wavelength, such as a superstructure grating, thermal tuning, or external cavity grating or vernier effects. Our tuning mechanism is to shift the pump stripe to different positions of an addressable chirped, location-dependent period grating to select the different lasing wavelengths. Interferometric lithography (IL) technique is used to pattern this chirped grating with two coherent spherical waves. A new grating fabrication optical arrangement that reduces the longitudinal chirp is discussed.

15. SUBJECT TERMS

Tunable infrared laser, distributed feedback laser, remote sensing, molecular spectroscopy

16. SECURITY CLASSIFICATION OF:			**17. LIMITATION OF ABSTRACT**	**18. NUMBER OF PAGES**	**19a. NAME OF RESPONSIBLE PERSON**
a. REPORT	**b. ABSTRACT**	**c. THIS PAGE**			Steven R. J. Brueck
U	U	U	UU	20	**19b. TELEPHONE NUMBER** *(include area code)* 505-272-7800

Abstract

An 80 nm continuous tuning range has been demonstrated on a large area index-coupled, optically pumped mid-infrared type-II semiconductor distributed feedback (DFB) laser, with a typical spectral linewidth of ~1.2 nm and 820 mW single facet output power. Different from other methods to widely tune the laser output wavelength, such as a superstructure grating, thermal tuning, or external cavity grating or vernier effects. Our tuning mechanism is to shift the pump stripe to different positions of an addressable chirped, location-dependent period grating to select the different lasing wavelengths. Interferometric lithography (IL) technique is used to pattern this chirped grating with two coherent spherical waves. A new grating fabrication optical arrangement that reduces the longitudinal chirp is discussed.

I. Introduction

The mid-IR 3–5 μm atmospheric transmission window is important for remote sensing and spectroscopic applications because it contains many fingerprint molecular absorption lines, such as C–H stretch at 3.3 μm. Many spectroscopic applications require a continuous wave (cw), single-longitudinal-mode (SLM), narrow linewidth, widely tunable, high-power laser source. In this report, we demonstrate an improved method to fabricate chirped grating and achieved stable grating normal configuration (GNC), real DFB lasing with successful F-P mode suppression over a tuning range of 80 nm.

II. Device Design and Fabrication

The gain medium which we used to demonstrate this tunable DFB laser is type-II InAs/InGaSb/InAs multiple W-quantum well (QW) structure grown on the GaSb:Te substrate (n=3.82) with molecular beam epitaxy (MBE). This material was supplied by Dr. Ron Kaspi (AFRL/DE). The three layer slab waveguide structure consists of GaSb top/bottom clad and the 1.5μm thick core layer (n=3.842), containing 14 mentioned QW's sandwiched with absorption layers optimized to fully and efficiently absorb the 1.908 μm pump laser power. The top clad is a 1.5μm thick GaSb (n=3.82) layer, in which we etch the chirped DFB grating.

Design of this DFB laser mainly needs to take account three constraints: adjusting the grating period to match the Bragg wavelength with the gain spectrum, centered at 3.06 μm at 77K; controlling of grating etch depth into the top clad of the slab waveguide structure to have sufficient mode confinement in the epitaxial direction to obtain enough modal gain for efficient lasing; determining the etch depth needed to give appropriate coupling strength for a given device cavity length (longitudinal dimension). Often times, there is a trade-off between the mode confinement factor and coupling coefficient. With all these considered, we decided to etch our chirped grating 500 nm deep into top clad layer, with a grating period in the range of about 410 to 420nm, 50% duty cycle is preferred for the maximum coupling coefficient. Dimensions of the DFB laser are set to 2.5×4 mm^2 in longitudinal and lateral directions, respectively. The longitudinal direction refers to the direction in which optical pump stripe is applied and the

lateral direction is the perpendicular direction across the pump stripe and parallel to the grating lines.

The chirped, position-dependent period grating is the key feature of our DFB laser to achieve tuning. To pattern this grating, IL techniques are used, with 355nm, 3rd harmonic ND-YAG laser as the coherent light source. A plano-convex lens in the exposure setup (Figure1.) converts the incident approximately planar wave into spherical waves to get the chirped grating.

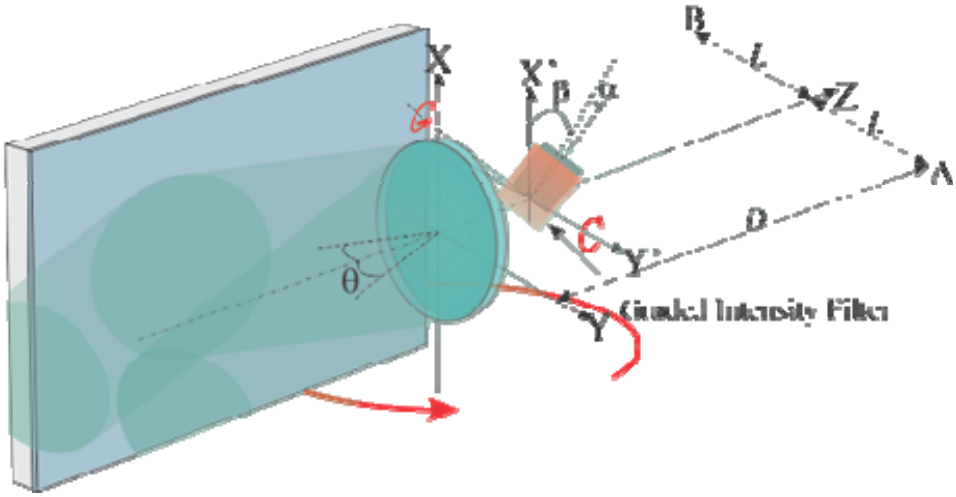

Figure 1. Interferometric lithography setup for quadratically chirped grating patterning

The interferometric lithography setup is shown in Figure 1. Basically, it is a Lloyd's mirror arrangement with an extra plano-convex lens (with the back flat surface in the (x,y) plane, and its optical axis in line with the overall optical axis) mounted perpendicular to mirror (in the (x,z) plane) as shown which converts incoming plane waves to spherical waves. At some distance behind the back surface of lens, but in front of the focal plane of the lens, we define another coordinate system (x',y') as shown. We need it to address the position and tilting of the photoresist coated die on which chirped grating is patterned. The semiconductor laser die is shown as the partially-obscured, tilted grey rectangle in Figure 1. The collimated coherent exposure beam comes from left side at an incidence angle of θ, chosen to produce the correct pitch based on the usual condition $p = \lambda/(2\sin\theta)$. For convenience of illlustration, the incident plane wave is separated and drawn in two portions with cylindrical cross-sections in the figure; in the actual set-up, a single large-area beam is used. One portion of the beam illuminates the lens directly. The other portion shines onto the mirror and is then reflected onto the lens. The two portions of the plane wave are incident on the front surface of the plano-convex lens with at angles of $\pm\theta$, symmetric with respect to the optical (z) axis of the optical system. After the lens there are two converging spherical waves, propagating along the original incidenct angles that

will focus at points A and B. The photoresist pre-coated die is placed in the overlap region of these two coherent converging spherical waves. In such a manner, a chirped interfering standing-wave pattern is formed and registered in the photoresist layer on the semiconductor die. With the above configuration, the separation of the two foci A and B is 2*L* and they are at a distance *D* behind the back surface of the lens. In the experimental arrangement, the plano-convex lens is 50 mm in diameter with a focal length of 51.5 cm at the 365 nm exposure wavelength.

This method of patterning grating will inherently generate grating with a spatially varying chirp on the die, characterized by both a lateral chirp (the period varies along the grating lines) and a longitudinal chirp (the period varies perpendicular to the grating lines). The chirp along the grating line direction named as lateral chirp is what provides DFB laser tunability. The longitudinal chirp affects the laser output and spectral linewidth performance and could cause mode hopping issues and must be controlled. If there is too much chirp in this direction, the DFB feedback will shift away from the lasing wavelength and only a part of the pumped stripe can contribute to the lasing. The goal of the optimization of chirped grating is to minimize the longitudinal chirp while still providing the maximum degree of lateral chirp and hence laser tuning. To enlarge lateral chirp with a low or tolerable longitudinal chirp, the photoresist coated die is intentionally tilted by rotating it around the *y*' axis at an angle β, relative to the optical axis. β, in this case is 45°. Also, we move the center of the die vertically off the optical axis along the *x*' direction to increase the lateral chirp. Additionally, the sample is rotated 6° azimuthally around its surface normal, indicated by α as shown in the figure. This tilts the grating lines relative to the cleaved facets of the semiconductor to suppress Fabry-Perot modes. The chirped grating period range across the sample as well as lateral and longitudinal chirp can be easily adjusted by changing lenses with different focal lengths, varying the incident angle θ, titling angle β, and shifting the sample off optical axis in the (*x*',*y*') plane. To compensate for the different light field intensity from the bottom over the area of the die due to the focusing, a graded intensity filter as show as the tilted orange box could be placed in front of die. This optical element was not used in our present experimental setup resulting in a noticeable variation of the grating duty cycle from the bottom to the top of die.

Grating period as a function of location by coordinates (*u*,*v*) on the die is derived as follows, assuming the incident beam is a plane wave. In this case, coordinate system used on die with which we derive the expression is built with origin is picked at the middle point the bottom edge of 10×10mm die, as shown in figure 2. The grating period calculation is done in the (*x*,*y*,*z*) coordinate system as seen in Figure 1, and then converted into the coordinate system (*u*,*v*) on the die with relation as shown as following.

$$\begin{aligned} x &= -u\cos\beta\sin\alpha + v\cos\beta\cos\alpha + C_x \\ y &= u\cos\alpha + v\sin\beta + C_y \\ z &= -u\sin\beta\sin\alpha + v\sin\beta\cos\alpha + C_z \end{aligned} \qquad (1)$$

Where β is the die titling angle and C_x, C_y are the offset of or origin of the (u,v) coordinate system in the (x',y') plane. C_z is the distance from the origin of the u-v coordinate system to the back surface of lens in Z direction. To simplify the expression for grating period, C_x and C_y are set to zero. Grating period as function of location on die is given by the following expression, taking into account the titling and azimuthal rotation of die.

$$\Lambda(u,v) = \frac{\lambda_0}{|\nabla m(u,v)|} = \frac{\lambda_0}{\sqrt{(\frac{\partial m}{\partial u})^2 + (\frac{\partial m}{\partial v})^2}} \qquad (2)$$

Where, m is an integer we used to indicate the optical path difference in terms of the multiple of the IL wavelength λ_0, from any location on the die to the two foci A and B behind the lens. Optical path different is given by the following expression.

$$m\lambda_0 = \sqrt{x^2 + (y+L)^2 + (D-z)^2} - \sqrt{x^2 + (y-L)^2 + (D-z)^2} \qquad (3)$$

In the above equation, L and D are the half separation of the foci and the distance of them from the back surface of the lens, respectively. These values are lens and incident angle dependent and calculated with Matlab program based on a ray-tracing algorithm. Contour of grating period on the die is plotted in Figure 2. Measured grating period will differ to some extent, compared with the value from the above expression due to reasons such as spherical aberration of lens, plane incident wave approximation and errors in die positioning and measurements.

The blue rectangle in the Figure 2(a) represents for the actual DFB device area which is $2.5\times4\text{mm}^2$. The blue rectangle in Figure 2(b) shows the grating period along the $u = 0$ line (center of the chip) on the real DFB device, which is covers the range from about 409- to 422-nm .The corresponding Bragg wavelength, also shown in the plot, is from 3060- to 3140-nm, assuming an effective index of 3.75. These results match very well with the measured device tunability.

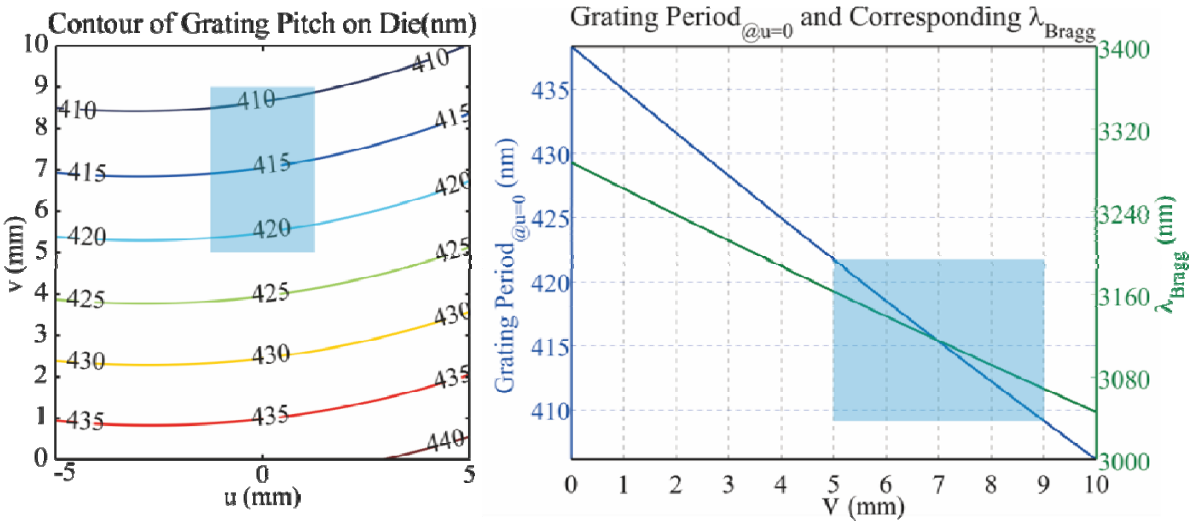

Figure 2. Left panel: Grating period contour as function of location on the die, with die tilting of 45 and azimuthal rotation of 6 taken into account. Right panel: Grating period along the line u=0 on die, and the corresponding Bragg wavelength are plotted. Blue rectangle in left panel shows the real device's dimensions of 2.5×4 mm^2, and the grating period range as well. The blue rectangle in the right panel gives the grating period range along $u = 0$ line and corresponding Bragg wavelength.

In reality, for a given lens to get to a target grating period range, we start with a guessed set of parameters and use the above calculation to get the incident angle θ and then adjust it to approach to the target range according to the grating period measurement conducted on a metrology setup up using an He-Ne laser.

Fabrication of the tunable DFB device follows very conventional procedures. We started with spin coating a 10×10 mm die with anti-reflection coating (ARC) and photoresist (PR). Then grating will be patterned in photoresist layer on die with IL. After that, grating pattern is transferred about 500nm into the top clad of slab waveguide structure with inductively coupled plasma (ICP), using BCl_3 plasma. Residual ARC and PR is removed using O_2 plasma with reactive ion etcher (RIE). In the next step, the die is lapped down to about 150 μm for better thermal conductivity. Then, a 2.5×4mm rectangle-shaped device is cleaved from the middle of the die as shown in figure 2(a), with dimensions in lateral and longitudinal direction respectively. The final step of device fabrication is indium bonding the device on to a gold coated copper heat sink mount to be mounted on the cold finger of liquid nitrogen Dewar. Longitudinal dimension is picked as 2.5 mm to compare with devices previously fabricated. Lateral dimension of 4 mm is chosen to avoid cracking of the device resulting from non-uniform thermal expansion under high power pumping.

III. Characterization of DFB Laser Operation

Due to the epitaxial structure design of the material system, this type-II gain medium only works up to about 100K. Because of that, all the characterization was conducted in liquid nitrogen (LN_2) Dewar at about 80K, including the output power, and spectral linewidth and tunability. The pump laser used in DFB laser characterization is a thulium fiber laser that has output of 20Watts at 1.908 μm with a collimated output beam diameter of about 5 mm. With a cylindrical lens, a pump stripe of about 100 μm wide is formed and projected perpendicularly onto DFB device mounted on cold finger of LN_2 Dewar. To avoid readjusting the output beam collection optics every time we shift the pump stripe to a new position on the device. We keep the pump beam/output collection optics fixed but mount the Dewar on a gear-reduced step motor driven translation stage. By shifting the stage, lateral scan across the while device is achieved equivalently. In such way, it significantly simplifies the whole characterization system. All the characterization is done with pump stripe perpendicular to the grating orientation, called grating normal configuration (GNC). Since the grating orientation is titled 6° relative to the facets, as shown in figure 3, pump stripe is not normal to the facets that Fabry-Perot modes are successfully suppressed. Also because the pump stripe is not normal to the facet, the output angle of the device is about 23° given by Snell's law.

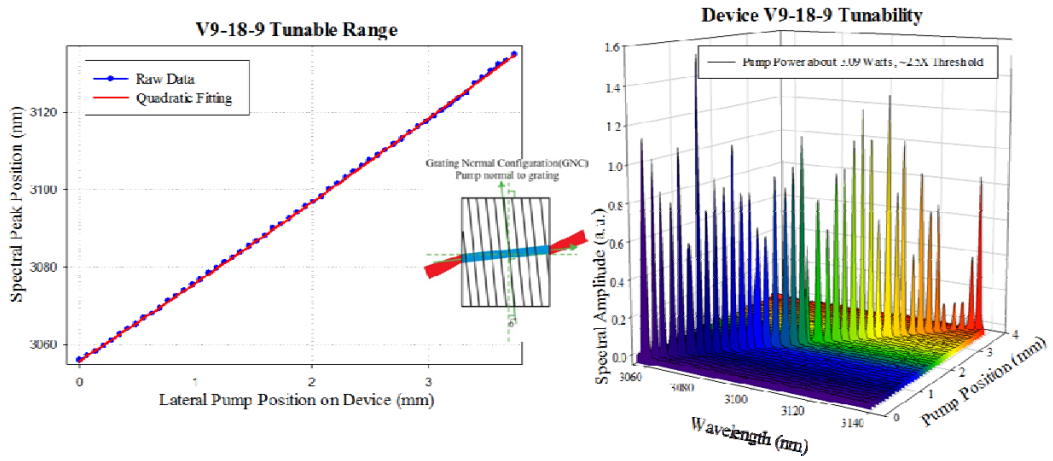

Figure3. DFB laser tunability Measurement In the Left panel, peak output wavelength as a function of pump stripe position is plotted in blue curve with data points marked. On top of it, the quadratic fitting of output wavelength is plotted in red line. The inset shows the grating normal configuration (GNC) used for the measurement. The right panel is a waterfall plot of the output spectra vs. pump position.

In the tunability demonstration, we shift the pump stripe position laterally across the whole device and acquire the spectrum at each position with monochromator. From the spectra at different positions on device, we extract information such as, spectral peak wavelength and linewidth. Spectral peaks are extracted from the spectra and plotted in left panel in Figure 3, as shown. This DFB laser device demonstrates a tunable range of 80nm, from 3057- to 3137-nm as

shown. Measured spectral peaks match very well with the quadratically fitted curve, with only a few spots off, jump from one side of fitting curve to the other. F-P modes are efficiently suppressed as shown in the waterfall plot on the right panel of figure 3.

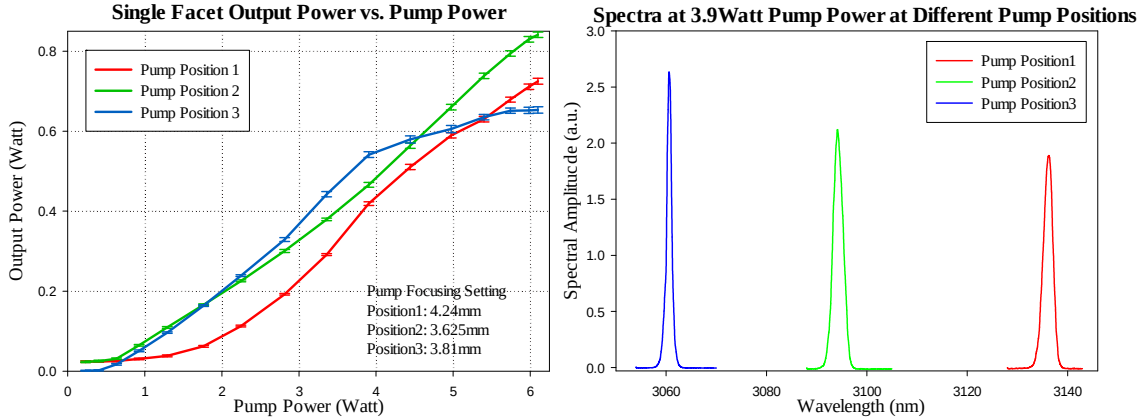

Figure 4. DFB laser output power Measurement. In the left panel, single facet output at three different pump positions is plotted with different colors. In the measurement, pump stripe focus was adjusted accordingly to maximize the output respectively. The right panel shows the spectra of the device at these different pump positions at the same pump power level of about 3.9 Watts.

The single facet output power of the DFB device is measured at three different positions and plotted in different colors as shown in figure 4 left panel. The output spectra of these three different pump positions are shown in the right panel with color coded. Threshold of these different pump positions are not exactly the same as shown in the figure, mainly due to the fabrication issues. As you can see the single facet output power of this device reaches about 820mW. And still does not show signs of rolling over. And the measured single facet output power is limited by the applied pump power.

The spectral linewidth of DFB laser output at about 2.5X threshold is plotted in figure 5. The data is the FWHM extracted directly from the spectra acquired at these different pump positions. Typical spectral line width of this device is about 1.2 nm is too wide for resolving Doppler broadened molecular lines at low pressure, but is ideal for application to atmospheric pressure gas remote sensing.

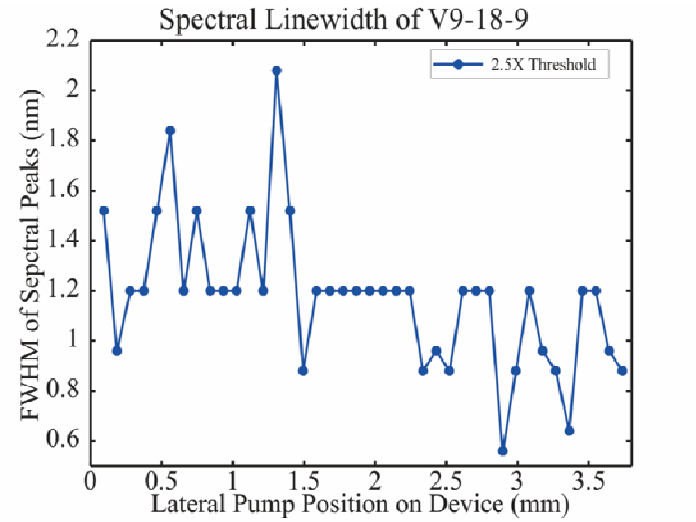

Figure 5. Spectral linewidth of DFB device output as wavelength tuning with pump power of about 2.5×threshold.

A very important characteristic of the tunable laser is to have continuous tuning. To further demonstrate the tunability, we instead used a F-P interferometer and tuned through multiple F-P orders. By measuring the transmittance of F-P interferometer with a high enough finesse, we can get the spectral line width and continuous tunability of output wavelength at the same time. When tuning the DFB laser device's output wavelength in the full range and measuring the F-P interferometer transmittance, we get 6 peaks as shown in the Figure 6, corresponding to six sequential F-P modes. Peak 6, appears as the pump stripe is shifted near the edge of the device where the lasing performance showed more instability. The cavity length of the F-P interferometer is fixed at about 365μm, with free spectral range of 411 GHz. Each data point in the plot corresponds to a pump stripe shift of 3.15 μm, equivalent to a wavelength change of 0.063- to 0.071-nm. This wavelength change is very small compared with the spacing of the F-P modes of the laser slab, which is of the order of 0.5 nm for the 2.5 mm longitudinal dimension. Considering the mirror reflectance of the external F-P interferometer is 0.985, the finesse is about 208. The smallest resolvable wavelength difference is same as the wavelength tuning step of 0.063 nm across the whole tuning range of DFB device. The spectral line width of the DFB laser is about 45GHz, which correlates with the value got by the FWHM measurement of the spectra by monochromator shown in figure 5. Multi-longitudinal mode operation was not observed in this device. Give all of the above, we think the sub-peaks showing on peak 3, 4 and 5 are real and mainly due to the existing lateral modes in laser output since the pump stripe is about 70 to 100 μm wide. In conclusion, we have achieved 80 nm of continuous tuning on a 4×2.5 mm^2 device.

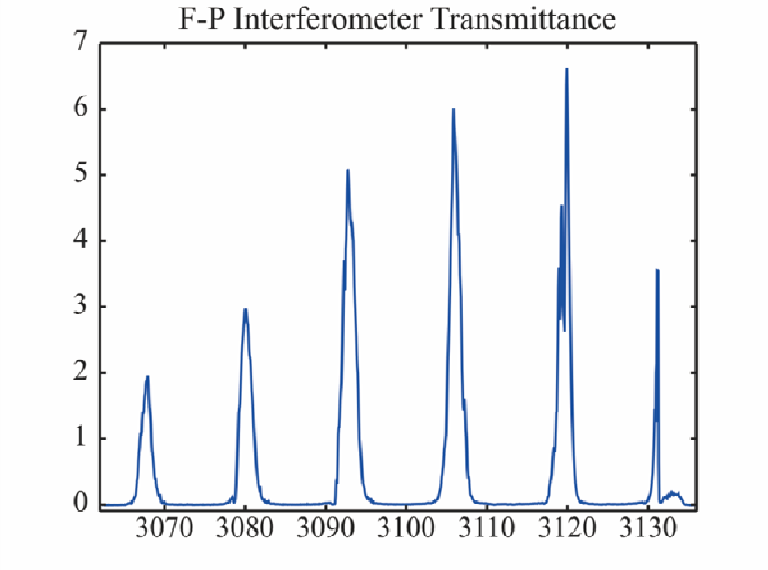

Figure 6. F-P Interferometer transmittance measurement with fixed cavity length while tuning DFB laser output wavelength.

IV. Discussion

In the left panel of figure 7, the average grating period along the u=0 line from bottom to the top on die is plotted as function of die titling angle in IL exposure in blue curve. Lateral chirp defined as the difference between maximum and minimum grating period divided by average grating period is plotted in green line. Likewise, in right panel of figure 7, the average grating period along the pump stripe across die as function of die tilting angle is plotted in blue. Longitudinal chirp along this pump stripe through the die center divided by average grating along the pump stripe is plotted in green. As an example for longitudinal chirp range on die, grating period along u=0 on die with 45° die titling and 6° azimuthal rotation is plotted in blue in figure 8. Longitudinal chirp along the GNC direction across the whole length of die is plotted in green. So based on these, if we further increase the die titling angle, we should get bigger lateral chirp for wider tunable range of easily over 100nm across a lateral dimension of 4mm. If we put more devices that from same die in series, we can further increase the laser tuning range with the limit from gain spectrum of gain medium. At the meantime as we increase the die titling angle in IL patterning, we should get even smaller longitudinal chirp along the pump stripe that impacts the laser performance. From figure 8, the trend of longitudinal chirp along GNC direction across the whole width of die shows a superlinear increase, we actually want to cleave the device from towards the bottom of the die for the reason of smaller longitudinal chirp, instead of from where we did as marked in figure 2 left panel.

But one thing need to be taken into account is as the tilting angle increases, the intensity variation from the bottom of the die to the top will increase, which will result in a grating duty cycle variation due to exposure dose differences. To resolve this issue, we need to put a graded

intensity filter in front of die as shown in figure (1) to get uniform field intensity over the die area during exposure.

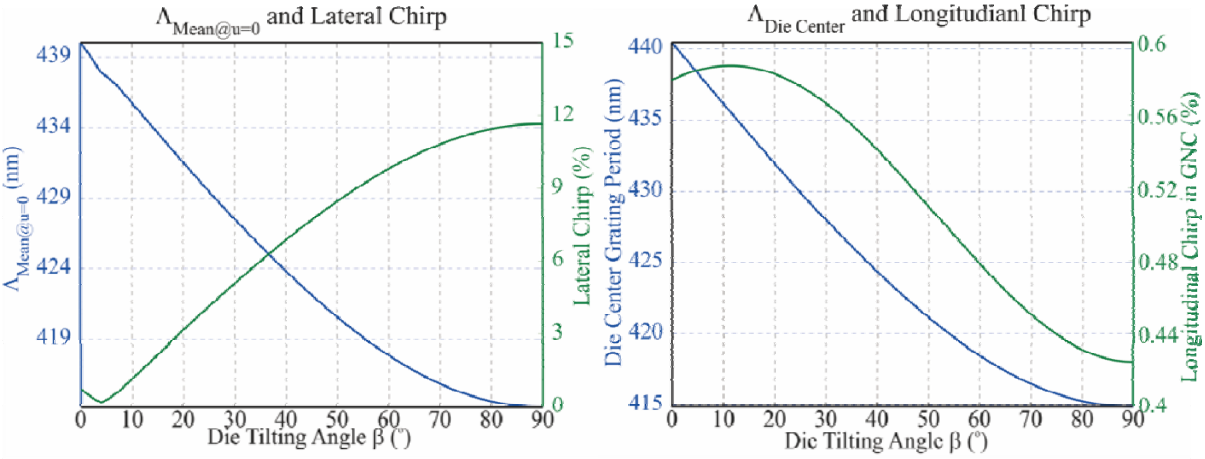

Figure 7. Grating periods along u=0 on die and Lateral Chip and longitudinal chirp as function of the die tilting angle in IL patterning. Die is 10×10mm.

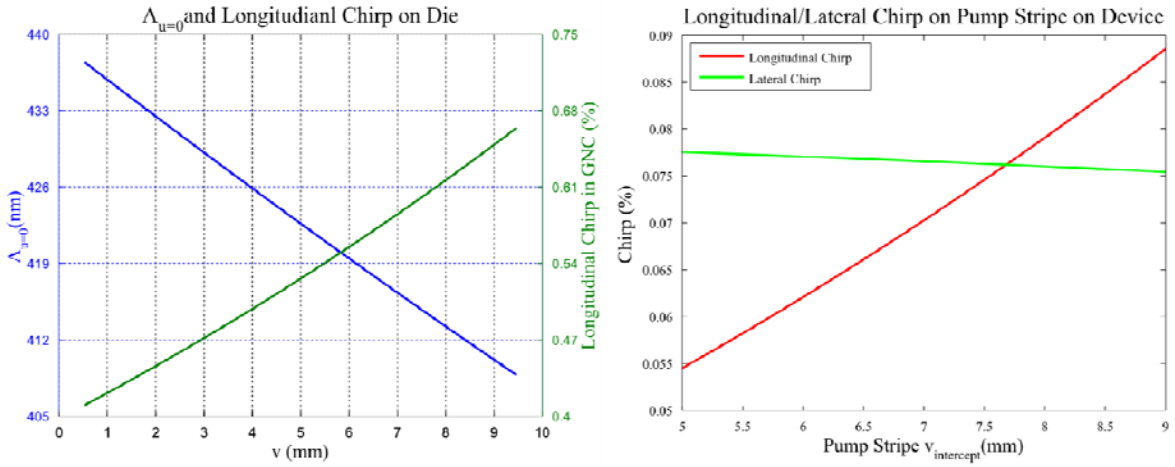

Figure 8. Grating period along u=0 on die and longitudinal chirp along the GNC direction across the whole width of die for the case when die tilting angle of 45° and azimuthal rotation angle of 6°. Right panel shows the lateral and longitudinal chirp on the pump stripe at different pump position on 2.5×4mm device cleaved from location shown on figure 2, assuming the pump stripe width is 100μm.

As shown in the characterization results, the spectral line width of the laser device is relatively large compared with other DFB lasers. This should be attributed to the quadratic chirp we have in the grating and to the presence of lateral modes in this gain, rather than index, guided structure. Considering the present DFB laser device has dimension of 2.5×4mm and the cleaving location from die, as shown in figure 2. The longitudinal chirp along GNC direction across the whole device is about 0.054-0.088% from bottom to top. Considering the pump stripe width is on the order of 100μm, across this width the lateral chirp stays at about 0.75% across the whole lateral length as shown in the right panel of figure 8. So, longitudinal and lateral chirp have the

comparable contribution to the chirp of grating period seen by pump stripe. The chirps in the grating period will be directly reflected by the output wavelength spectral linewidth.

In summary, based on laser experimental results, chirp has a very strong effect to laser behavior. From an application standpoint, we would like largest possible lateral chirp for the widest tunable range. But due to the existence of chirp, it increases the local, position dependent and reflection parameters of the local grating also shift and there can be a loss of reflectance as the local reflection band is shifted away from the lasing wavelength. Along the whole length of pump stripe, the different grating periods at different locations contribute to different Bragg wavelengths. Together with the fact that across the full with pump stripe in lateral direction, the lateral chirp gives different grating periods. Overall effects from these factors lead to a relatively wider spectral line width as shown in the characterization section. For longitudinal chirp, one way of explanation is that not all the grating along the pump stripe will contribute to the lasing wavelength that the effective cavity length is shorter that the coupling strength is lower than the case with straight grating and same cavity length. In addition, the tilt of the grating facets along the pump stripe, associated with lateral chirp will result in and extra loss. Other than mentioned above, increasing chirp decreases the stop band width, increases the depth of adjacent lopes (related to side mode suppression ration too) and alters the reflected phase as well. The undergoing simulation is trying to correlate all these to the performance of the present type of laser.

V. Conclusion

A new method of fabricating chirped grating by interference between two spherical waves was developed based on interferometric lithography (IL) with 355 nm 3rd harmonic of Nd YAG laser. Index coupled DFB laser with this chirped grating is fabricated. A 4×2.5mm^2 device has grating period range of 410- to 420-nm, corresponding to a tunable lasing range of 3060-to 3140-nm with effective refractive index of ~3.75 under a 2.5× threshold pumping condition. All the characterization was done in grating-normal pumping mode with successfully suppression of F-P modes, as shown in the figures.

It is important to note that by increase the tilt angle of the sample, we can further increase the lateral chirp to get a wider tunable range with even lower longitudinal chirp. This makes a tunable range of over 100 nm or more feasible for a 4mm wide tunable DFB device.

In conclusion, we have developed a novel method to fabricate chirped grating for type-II optically pumped tunable DFB laser with 80nm continuous tunable range and 820 mW pump-limited single facet output power. This is an ideal light source for applications such as atmospheric pressure stand-off gas sensing.

Publications:

Xiang He, R. Kaspi and S.R.J. Brueck, *Optically Pumped Type-II Mid-IR Tunable DFB Laser*, Proc. SPIE **8277**, 82771C (2012).

Patents awarded:

7,656,912 S. R. J. Brueck, L. Xue and R. Kaspi, *Tunable infrared lasers for gas-phase spectroscopy* (issued 2/2/2010)

Patents pending:

13/843,332 Method and Apparatus for Fabrication of Controlled Chirp Gratings
Filed: 3/15/13 Xiang He, S. Benoit and S.R.J. Brueck

Optically pumped type-II Mid-IR tunable DFB laser

Xiang He*[a], R. Kaspi[b] and S. R. J. Brueck[a]
[a]Center for High Technology Materials, University of New Mexico, Albuquerque, NM 87106;
[b]Air Force Research Laboratory, Directed Energy Directorate, Kirtland Air Force Base, Albuquerque, NM 87117

ABSTRACT

A new approach to tunable mid-infrared lasers, an optically pumped, type-II, InGaSb/InAs gain medium with a chirped distributed feedback grating, has been developed. The chirped grating is patterned using an interferometric lithography (IL) technique with spherical wave fronts and etched into the top cladding of the laser slab waveguide structure. Because the period of grating increases gradually laterally, wavelength tuning is implemented by shifting pump stripe to different positions on the device with different grating periods. Fabry-Perot modes from the cleaved facets are successfully suppressed by fabricating the grating 6° tilted with respect to facets and adjusting the pump stripe normal to the grating. Continuous tuning of 30 nm around 3.1 μm with 320 mW single facet output power at 80K and a 1.6 nm FWHM is reported. The present device is designed in the 3- to 4-μm range which matches a low loss atmospheric transmission window, and covers an important region of molecular vibration spectra, in particular, the hydrocarbon C-H stretch at ~ 3.3 μm, making it suitable for atmospheric pressure remote gas sensing of industrially important small molecules such as methane, hydrogen chloride and ammonia.

Keywords: Tunable, DFB, Mid-IR, Semiconductor Laser, interferometric lithography, chirped grating,

1. INTRODUCTION

Mid-infrared (Mid-IR) semiconductor lasers have achieved significant advances in performance over the past decade. Generally, there are three major types of high performance mid-IR semiconductor-based lasers: electrically pumped intersubband quantum cascade (QC) lasers,[1-4] electrically pumped interband cascade (IC) lasers,[5-9] and optically pumped interband lasers.[11-16] With the exception of the QC lasers, these mid-IR type-II lasers are based on the "W" shaped InAs and InGaSb quantum well structure, first proposed by Meyer *et al.*,[10] shown in Fig. 1a). The "W" shape takes its name from the pattern of the alignment of the different quantum well layers of different materials as shown.[17]

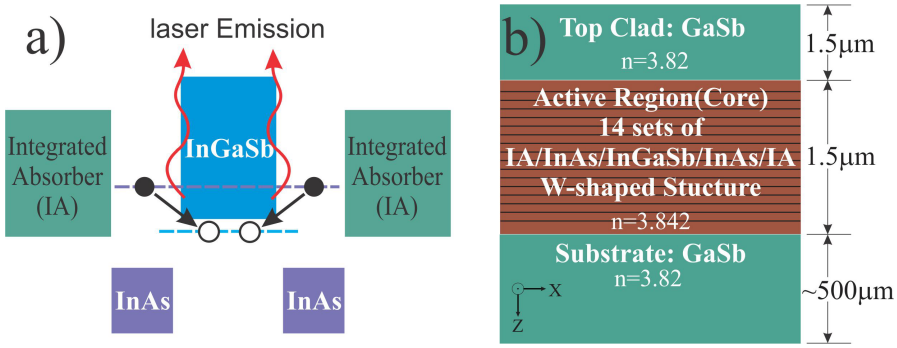

Figure 1. a) Generic epitaxial structure design for optically pumped semiconductor laser. The alignment of the energy bands of the different material layers forms a "W" shaped pattern. The purple and blue dashed lines represent the effective conduction and valence band edges. The solid and open circles stand for electrons and holes respectively. b) Cross section view of the structure of our laser device. In the core layer of the slab waveguide, there are 14 sets of the W-shaped structure shown in a) to fully absorb the pump laser power.

*xianghe@unm.edu; phone 1 505 272-7920; fax 1 505 272-7801

Novel In-Plane Semiconductor Lasers XI, edited by Alexey A. Belyanin, Peter M. Smowton,
Proc. of SPIE Vol. 8277, 82771C · © 2012 SPIE · CCC code: 0277-786X/12/$18 · doi: 10.1117/12.909033

QC lasers have the advantage of room temperature operation with several hundred mW output power but their output power drops as temperature increases. One of the critical drawbacks of QC lasers is that the efficiency drops rapidly as the output wavelength becomes shorter than ~4.5 μm, making them unsuitable for the important 3- to 5-μm atmospheric window. For the mid-IR range, IC lasers do not achieve high power output with electrical pumping. In comparison, optically pumped type-II IC lasers uniquely provide multi-Watt, continuous-wave, narrow linewidth operation in the important atmospheric transmission widow range of 3- to 4.5-μm. They are suitable for applications in remote gas sensing, absorption vibration spectroscopy and mid-IR countermeasures. This paper provides details on a novel approach to an optically pumped, rapidly, widely and continuously tunable, mid-IR DFB laser.

By varying the thickness of the InAs layer, type-II semiconductor lasers cover the range from ~2.3- to 12-μm, including the bulk of the molecular fingerprint spectral region. The laser presented in this paper is an optically pumped type-II tunable DFB laser, operating continuous-wave (CW) with a single longitudinal mode (SLM), a narrow spectral linewidth, high output power, a wide and continuous tuning range and good beam quality. All these features make it a suitable candidate for application to remote sensing for gases such as methane and ammonia in the mid-IR and nerve gases in the LWIR.

Fig. 1b) shows the cross section view of epitaxial structure of the wafer. The slab waveguide structure is grown on a GaSb wafer. In the core of the waveguide, there are 14 sets of integrated absorber-InAs/InGaSb/InAs-integrated absorber structures, evenly distributed across the total thickness of 1.5μm which is designed so to fully absorb the pump power and allows fundamental transverse mode to lase. The integrated absorber is composed of $(GaSb)_x(InAs_{0.89}Sb_{0.11})_{1-x}$, lattice matched and band adjusted to uniformly absorb the 1.908 μm pump laser power. The effective refractive index in the core layer is only 0.02 higher than in the clad layers, providing a low confinement factor that has better beam quality and suppresses filaments.[18-19]

2. METHODOLOGY

Our approach to achieve a mid-IR tunable DFB laser is novel compared with the traditional tunable lasers based on DFB thermal tunability, external cavities with a grating mirror,[20-23] or Vernier-effect DFB lasers with super structured grating.[24-25] These designs achieve tunability either by changing the temperature and refractive index that requires or by using a frequency selective the grating. Thermal tuning is slow and restricted to small wavelength ranges. External cavity grating approaches require precise alignment and large, heavy vibration isolation approaches.

Our laser is an index-coupled DFB laser which means the grating is only fabricated in the clad layer. In the design of this laser, there are mainly three constraints we need to address: the grating period; the coupling strength; and the transverse mode profile. First, the grating period needs to be within the gain spectrum of the active region, in this case centered at about 3.06 μm at 80 K. By Bragg equation, the grating period should be in the vicinity of the 419 nm, given that the effective refractive index is about 3.71.

$$\lambda_{Bragg} = 2n_{effiective}\Lambda \tag{1}$$

Where λ_{Bragg} is the Bragg wavelength, $n_{effective}$, the modal index and Λ is the grating period. Second, the coupling strength κL should be in a range between 1 to 3 to give proper feedback without introduction of spatial hole burning phenomena.

$$\kappa\mathcal{L} = \frac{2\,|\,\bar{n}_1 - \bar{n}_2\,|}{(\bar{n}_1 + \bar{n}_2)\Lambda}\mathcal{L} = \frac{\Delta\bar{n}}{\bar{n}\Lambda}\mathcal{L} = \frac{2\Delta\bar{n}}{\lambda_{Bragg}}\mathcal{L} \tag{2}$$

Where κ is the coupling coefficient and $\bar{n}_{1,2}$ correspond to the effective index of the top or groove segment of the grating in the top clad, and $\mathcal{L}$ is the cavity length. The equation is for the simple case of a straight grating with 50% duty cycle. For tunability, the grating period Λ is a function of the location on device. Third, the optical confinement of the laser should be above 0.35 but not so high as to compromise the output beam quality and result in filamentation at high pump levels. Using standard DFB laser design rules, the optimum grating depth in the top clad is determined to be 500 nm. Modal index and optical confinement factor in the design of this laser are calculated with online optical simulation software LIGHTS[26] by Dr. Andrew Sarangan at University of Dayton.

Instead of fabricating a uniform grating to select the operational wavelength of laser, we made a quadratically chirped grating using an interferometric lithography (IL) technique by interfering two spherical wavefronts. The experimental setup for IL is shown in Fig. 2. In the Fig. 2a), the collimated 3rd harmonic output of a Nd:YAG laser at 355 nm is incident from the left hand side. Half of the beam directly illuminates the plano-convex lens, the other half is reflected from the Lloyd's mirror onto the lens. The lens converts the planar wavefronts to spherical wavefronts that are focused to the two virtual foci A, and B. L is the separation of the two foci and D is their distance to the back surface of the lens, both are incident angle θ dependent and graphically solved with Matlab program based on simple ray tracing. To avoid Fabry-Perot (F-P) modes in the laser output, we rotate the die/sample 6° as shown in the figure 2b) to tilt the grating orientation. In this way, when we adjust the pump stripe to be normal to the grating, the F-P modes are successfully suppressed as shown in lasing results.

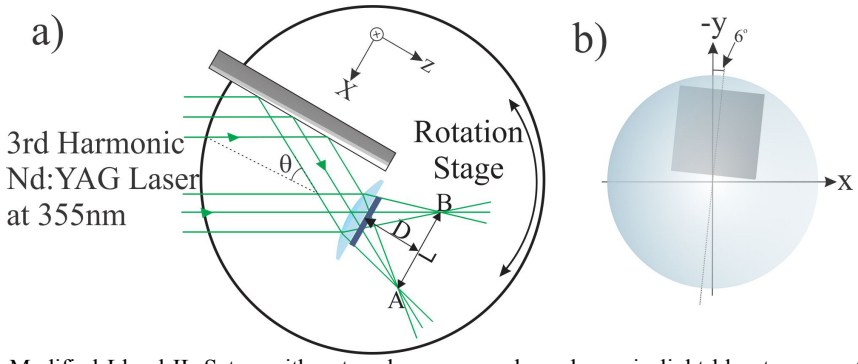

Figure 2 a) Modified Lloyd IL Setup with extra plano-convex lens shown in light blue to convert the planar wave fronts of incident beams to spherical and converges them to two virtual foci A, B behind photoresist coated die shown in dark blue. b) The die is rotated clockwise 6° to make grating tilted with respect to the edge as shown by the gray square.

The grating period on the DFB laser as a function of the coordinates and IL laser wavelength and the location of the two virtual foci is given by the equation:

$$\Lambda(x,y)=\frac{\lambda_{IL}}{\dfrac{x+L/2}{\sqrt{(x+L/2)^2+D^2+y^2}}-\dfrac{x-L/2}{\sqrt{(x-L/2)^2+D^2+y^2}}} \tag{3}$$

Where *x, y* are the coordinates on the die. A grating period contour plot including the 6° tilt to the facets is shown in Fig. 3a).

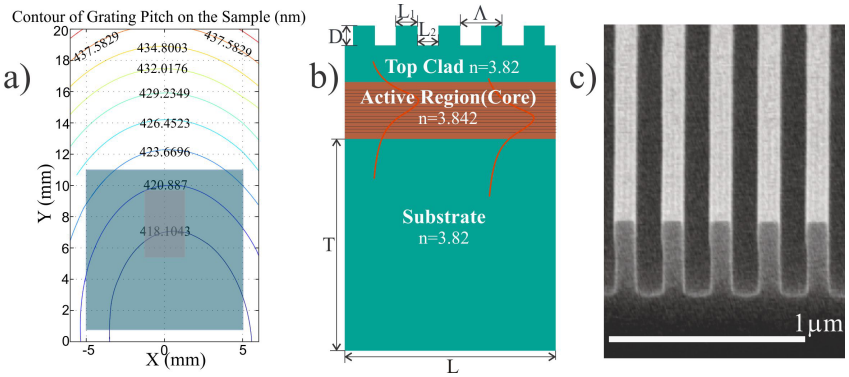

Figure 3. a) Contour plot of the grating pitch as function of location in a 12×20mm zone, for the case of die rotated 6°. The blue square corresponds to the 10×10mm die got from AFRL lab and the grey rectangle represents the 2.5×4 mm^2 DFB device cleaved out from the die. b) Cross section view of the device. Grating period of Λ~419 nm is etched into the top clad for D = 500 nm. Substrate is thinned to T~150 μm for better thermal conduction. c) SEM picture taken of the grating etched into top clad of device.

Once the grating is patterned in the photoresist, the pattern is transferred into the top of laser's slab waveguide structure shown in Fig. 3b), c) using an inductively coupled plasma (ICP). The grating etch depth into top clad is 500 nm as designed. In figure 3c) shows a SEM picture of the grating after ICP etch. Then the die is thinned down to about 150 μm and a 4×2.5 mm^2 DFB device is cleaved from the center of the die as shown as the gray rectangle in figure 3a). 4 mm is the lateral dimension of the device, which is picked to give as wide as possible tunable range without cracking issues from non-uniform thermal expansion due to local heating by the pump laser. 2.5 mm is the cavity length picked to give proper coupling strength, also allowing comparison with previously made devices with the same dimension. The final step (Fig. 4a) is indium mounting the device onto a copper heat sink and then to the cold finger of liquid nitrogen Dewar.

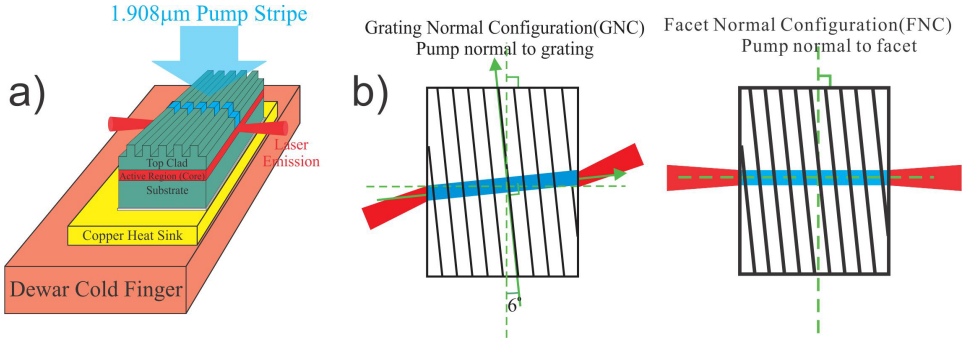

Figure 4. a)Pumping geometry for laser characterization. Device is indium mounted on to a copper heat sink then screwed onto the cold finger of liquid nitrogen Dewar. b) Two different pumping configurations: GNC, pumping normal to the grating; FNC, pumping normal to the facets.

In characterization, a thulium fiber laser at 1.908 nm wavelength is chosen to be the pump laser. Pump stripe is formed with a CaF_2 cylindrical lens. Benefiting from the flexibility of optical pump, we can rotate the cylindrical lens to adjust the pumping stripe's direction to either perpendicular to the cleaved facets [facet normal configuration (FNC)] or perpendicular to the grating orientation [grating normal configuration (GNC)], as shown in Fig. 4b). The output beam is coupled into a monochromator or Fabry-Perot interferometer together with InSb detector for spectral measurement or into a power meter for output power measurement. Since we have a varying grating period on the device, by shifting the device in lateral direction with pump beam fixed, we pump a different grating period and hence have a different output wavelength.

3. RESULTS

Grating normal configuration is the preferred operation configuration, since it successfully suppresses the F-P modes as shown in the plots. All the results shown herein were acquired in GNC. We did operate the laser in FNC for comparison. The device operates in a DFB mode only under a certain pump power, for higher pump power the F-P modes appear in the spectrum and eventually dominate the output spectrum as the pump power is further increased. When the device operates in FNC mode under DFB control, the output wavelength is given by equation (1) with an extra factor of cos(β), where β = 6°, corresponds to the titling of the grating orientation with respect to the facets. The other issue of this configuration found in the previously fabricated device is the impact from F-P modes in the composite grating/edge reflector cavity. During wavelength tuning, the spectral peak of the output emission jumps from one F-P mode to the neighboring modes, so the tuning is not continuous. Because of the long cavity length, 2.5 μm, the longitudinal mode spacing is less than a pressure broadened molecular linewidth, so all molecular lines are observed.[16]

All the characterization is at 80K. The device shows about 30 nm of continuous tuning around 3.08 μm as shown in Fig. 5. The device does not lase at both top and bottom edges of the chip, probably due to defects from cleaving. Single facet output power is also measured as function of the pump power. The output power is limited by the available pump power, without any evidence of saturation. Together with Fig. 6, we can conclude that within the whole pump power range, DFB laser operates stably with a single longitudinal mode; the F-P modes are successfully suppressed.

In figure 5a), the blue dots are the experimental data and the red curve is the quadratic fitting of the data to the theoretical expectation of the lasing wavelength from Eq. 3. The experimental data agree with theory fairly well; however, there are a few jumps of the lasing wavelength showing output wavelength changes above or below the theoretical expectation, and sometime device lases on either side of the theoretical value. This is likely due to the degeneracy of DFB modes, and interaction with the longitudinal chirp of the grating, this will be discussed more fully elsewhere. To address this problem, we plan to deposit metal into the grooves of the grating, to introduce asymmetric loss and favor a single longitudinal mode. The waterfall plot in figure 5. shows that across the whole tunable range, the device operates in single longitudinal mode. The F-P modes have been suppressed successfully.

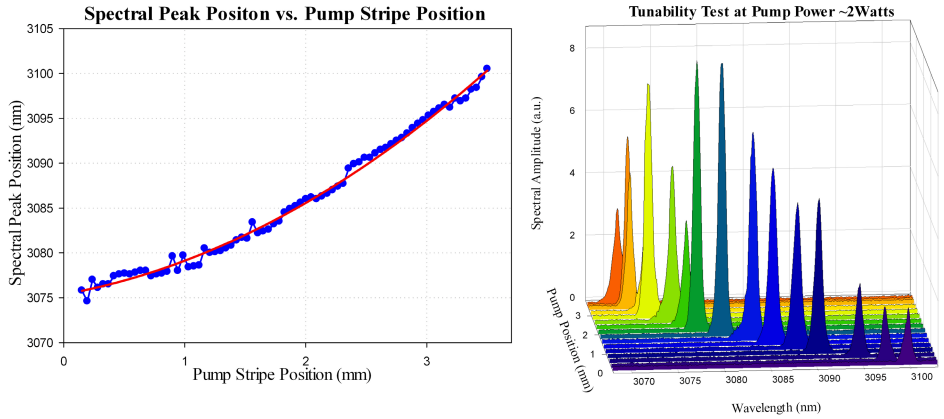

Figure 5. Left: Plot of tunability of the DFB device at 2W pump power, about ~2X threshold. The blue dots are the experimental data and the red curve is the quadratic fitting. Right: Waterfall plot of the spectral at different pump positions, at about 2X threshold of 2W pump powers.

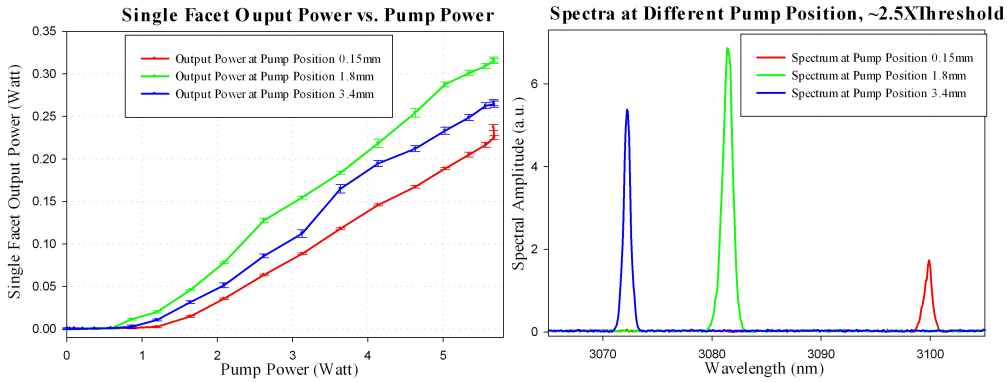

Figure 6. Left: A plot of output power as function of pump power at three different pump stripe positions. Right: Spectra at these three pump positions.

The linewidth of this device is about 1.6 nm at the pump power of about 2×threshold. This is large compared with typical low-power, narrow stripe, index guided DFB lasers. The main reasons include: a) the grating patterned with our method varies along the pump stripe as well as transverse to the stripe (the tuning direction). Different grating periods along the stripe will select different lasing wavelength which will broaden the overall line width of the laser output. b) Considering the pump stripe is about 100μm wide, across it the grating periods varies due to the lateral chirp which broadens the line width of the laser output as well though longitudinal chirp here is dominant reason for wide line width. The longitudinal chirp and lateral chirp are coupled in our approach of the grating patterning and they also depend on the focal length of the plano-convex lens used in IL and the incident angle of the interfering beams. Present value for longitudinal chirp for this device along the pump stripe is about 0.1% which restricts the effective laser length and impacts the line width.

4. CONCLUSION

We report a novel technique for the implementation of a mid-IR type-II tunable DFB laser. The present device shows about 30 nm continuous tunable range around 3.1 μm with a single-facet output power of about 320 mW (Fig. 6) and a line width of about 1.6 nm. These characteristics make this laser a suitable candidate for atmospheric pressure spectroscopy. Taking into account the atmospheric transmission windows, this technique is applicable to the remote gas sensing applications for light molecules such as methane, ammonia and hydrogen chloride in 3 to 5μm range. Extending the dimensions of the device to 10 mm, would give a tunable range on the scale of the laser gain bandwidth of about 200 nm. This would make it possible to resolving multiple spectral lines of multiple target molecules that very convenient for identification of the molecules. Also as mentioned previously, by varying the thickness of InAs layer in this type-II material system, gain spectral could cover in the range from 2 to 12μm. The technique demonstrated in this paper will be useful for spectroscopy applications from across the entire IR molecular fingerprint region.

ACKNOWLEDGEMENT

Support for this work was provided by DTRA under contract DTRA01-03-D-0009-0026, by AFOSR, and by and ARO-SBIR grant under subcontract from Southwest Sciences, Santa Fe, NM.

REFERENCES

[1] J. Faist, F. Capasso. D. L. Sivcok Cl Sirtori, A. Hutchinson, and A. Y. Cho, "Quantum cascade laser,", Science **264**, 553-556 (1994).
[2] A. Evans, J. S. Yu, S. Slivken, and M. Razeghi, "Continuous-wave operation of λ ~ 4.8 μm quantum-cascade lasers at room temperature," Appl. Phys. Lett. **85**, 2166-2168 (2004).
[3] Q. Yang, W. Bronner, C. Manz, R. Moritz, Ch. Mann, G. Kaufel, K. Köhler, and J. Wagner, "Continuous-wave operat ion of GaInAs–AlGaAsSb quantum cascade lasers," IEEE Photon. Technol. Lett. **17**, 2283-2285 (2005)
[4] Q. Yang, C. Manz, W. Bronner, Ch. Ma nn, L. Kirste, K. Köhler, and J. Wagner, "GaInAs/AlAsSb quantum cascade lasers operating up to 400 K," Appl. Phys. Lett. **86**, 131107 (2005).
[5] R. Q. Yang, "Mid-infrared interband cascade lasers based on type-II heterostructures," Microelectron. J. **30**, 1043-1056 (1999).
[6] J. L. Bradshaw, J. D. Bruno, J. T. Pham, D. E. Wortman and R. Q. Yang, "Continuous wave operation of type-II interband cascade lasers," IEE Proc. Optoelectron. **147**, 177-180 (2000).
[7] R. Q. Yang, J. L. Bradshaw, J. D. Bruno, J. T. Pham, and D. E. Wortman, "Mid-infrared type-II interband cascade lasers," IEEE J. Quant. Electron. **38**, 559-568 (2002).
[8] K. Mansour, Y. Qiu, C.J. Hill, A. Soibel and R.Q. Yang, "Mid-infrared interband cascade lasers at thermoelectric cooler temperatures," Electron. Lett. **42**, 1034-1035 (2006).
[9] M. Kim, D. C. Larrabee, J. A. Nolde, C. S. Kim, C. L. Canedy, W. W. Bewley, I. Vurgaftman, and J. R. Meyer, "Narrow ridge interband cascade laser emitting high CW power," Electron. Lett. **42**, 1097–1098 (2006).
[10] J. R. Meyer, C. A. Hoffman, F. J. Bartoli, and L. R. Ram-Mohan, "Type-II quantum-well lasers for the Mid-wave length infrared," Appl. Phys. Lett. **67**, 757-759 (1995).
[11] A. K. Goyal, G. W. Turner, H. K. Choi, P. J. Foti, M. J. Manfra, T. Y. Fan, and A. Sanchez, "High-efficiency optically pumped Mid-IR lasers with integrated absorbers," Proc. IEEE LEOS **1**, 249-250 (2000).
[12] R. Kaspi, A. Ongstad, C. Moeller, and G. C. Dente, "Optically pumped integrated absorber 3.4μm laser with InAs-to-InGaAsSb type-II transition," Appl. Phys. Lett. **79**, 302-304 (2001).
[13] R. Kaspi, A. Ongstad, G. C. Dente, J. Chavez, M. L. Tilton, and D. Gianardi, "High power and high brightness from an optically pumped InAs/InGaSb type-II Mid-infrared laser with low confinement," Appl. Phys. Lett. **81**, 406-408 (2002).
[14] R. Kaspi, A. P. Ongstad, G. C. Dent e, J. R. Chavez, M. L. Tilton, and D. M. Gianardi, "High performance optically pumped antimonide lasers operating in the 2.4-9.3 μ m wavelength range," Appl. Phys. Lett. **88**, 041122 (2006).
[15] Liang Xue, S.R. J. Brueck and R. Kaspi, "High-power continuous-wave single-longitudinal-mode operation of an optically pumped DFB laser at λ~3.64 μm," Photon. Tech. Lett. **20**, 727 (2008).

[16] Liang Xue, S. R. J. Brueck and R. Kaspi, "Widely tunable distributed-feedback lasers with chirped gratings," Appl. Phys. Lett. **94**, 161102 (2009).
[17] A. Krier (Ed.), [Mid-infrared Semiconductor Optoelectronics], Springer-Verlag London Limited, 189-218 (2006)
[18] G. C. Dente, "Low confinement factors for suppressed filaments in semiconductor lasers," IEEE J. Quant. Electron. **37**, 1650-1653 (2001).
[19] R. Kaspi, A. Ongstad, G. C. Dente, J. Chavez, M. L. Tilton, and D. Gianardi, "High power and high brightness from an optically pumped InAs/InGaSb type-II Mid-infrared laser with low confinement," Appl. Phys. Lett. **81**, 406-408 (2002).
[20] M. Ito and T. Kimura, "Oscillation properties of AlGaAs DH Lasrs with an external grating," IEEE J. Quant. Electron. **QE-16**, 69-77 (1980).
[21] R. Wyatt, W. J. Devlin, "10 kHZ Linewidth 1.5 mm InGaAsP External cavity laser with 55 nm tuning Range," Electron. Lett. **19**, 110-112 (1983).
[22] B. Glance, C. A. Burrus, and L. W. Stulz, "Fast frequency-tunable external-cavity laser," Electron. Lett. **23**, 98-100 (1987).
[23] Y. Hori, H. Asakura, F. Sogawa, M. Kato, and H. Serizawa, "External-cavity semiconductor laser with focusing grating mirror," IEEE J. Quant. Electron. **26**, 1747-1755 (1990).
[24] Todt, R., Jacke, T., Meyer, R., Adler, J., Laroy, R., Morthier, G., Amann, M.-C., "Sampled grating tunable twin-guide laser diodes with over 40-nm electronic tuning range," IEEE Photon. Technol. Lett. **17**, 2514-2516 (2005).
[25] Jens, Buus, Markus-Christian Amann, Daniel J. Blumenthal, [Tunable Laser Diodes and Related Optical Sources] 2nd Edition, Wiley-IEEE Press, 169-211 (2005).
[26] www.nano-fab.com/lights/.